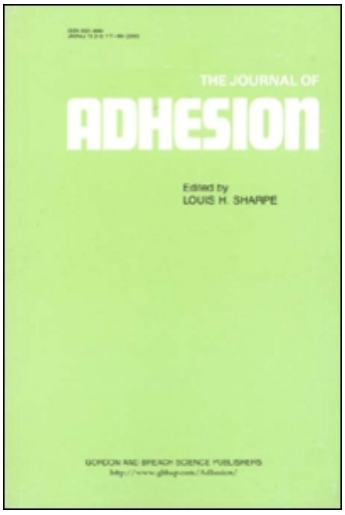

The Journal of Adhesion
Publication details, including instructions for authors and subscription information:
http://www.informaworld.com/smpp/title~content=t713453635

Strength of adhesive joints with adherend yielding: II. Peel experiments and failure criteria

R. X. Wang[a]; A. N. Sinclair[a]; J. K. Spelt[a]
[a] Department of Mechanical and Industrial Engineering, University of Toronto, Toronto, Ontario, Canada

Online publication date: 08 September 2010

To cite this Article Wang, R. X. , Sinclair, A. N. and Spelt, J. K.(2003) 'Strength of adhesive joints with adherend yielding: II. Peel experiments and failure criteria', The Journal of Adhesion, 79: 1, 49 — 66
To link to this Article: DOI: 10.1080/00218460309558
URL: http://dx.doi.org/10.1080/00218460309558

The Journal of Adhesion, 79: 49–66, 2003

0021-8464/03 $12.00 +.00
DOI: 10.1080/00218460390147915

Taylor & Francis
Taylor & Francis Group

STRENGTH OF ADHESIVE JOINTS WITH ADHEREND YIELDING: II. PEEL EXPERIMENTS AND FAILURE CRITERIA

R. X. Wang
A. N. Sinclair
J. K. Spelt
Department of Mechanical and Industrial Engineering,
University of Toronto, Toronto, Ontario, Canada

Peel tests were conducted with an epoxy adhesive on nine rigid-flexible peel configurations: combinations of 1, 2, and 3 mm aluminum adherend thickness and 30°, 60°, and 90° peel angle. The peel model described in an accompanying paper was used to calculate the stress and strain distributions in the adhesive, the strain energy release rates, and the root curvature of the adherend corresponding to steady-state peel failure. Two failure criteria were examined: the critical von Mises strain and the critical fracture energy, G_c. The first criterion was found to be essentially independent of the peel angle but dependent on the thickness of the peel adherend. It produced predictions of the peel force that had an average error of 11%. The fracture energy criterion showed that G_c depended on the average phase angle of the loading. This criterion was preferred, having an average prediction error of 6% over the nine experimental cases, and requiring fewer free parameters.

Keywords: Peel strength; Failure criteria; Adherend yielding

INTRODUCTION

The failure of adhesive joints with relatively weak adherends is often accompanied by extensive plastic deformation of the adherends. A common example is the typical peel test. In such cases, the

Received 20 March 2002; in final form 8 July 2002.

The work was supported by the Centre for Automotive Materials and Manufacturing. The support of Henkel Corp., Essex Specialty Products Inc., and Alcan International Ltd. is also gratefully acknowledged.

Address correspondence to J. K. Spelt, Department of Mechanical and Industrial Engineering, University of Toronto, 5 King's College Road, Toronto, Ontario, Canada M5S 3G8. E-mail: spelt@mie.utoronto.ca

identification of a failure criterion and the ability to predict joint strength are complicated by the strong connection between the adhesive stress state and the deformed adherend geometry in the vicinity of the peel root where the adhesive is breaking. Crocombe and Adams [2] used an elasto-plastic finite element model to investigate a strain-based adhesive failure criterion in peel tests with aluminum adherends. The critical plastic strain proved to be dependent on the yield strength of the adherend [2]. Fracture criteria, typically involving the critical energy release rate and phase angle, have also been considered; see, for example, Kinloch et al. [3] and Moidu et al. [4]. Recently, a cohesive zone model has been used with some success to analyze adhesive joints with yielding adherends [5–7].

In our earlier research [1], the analysis of an adhesive sandwich element was described and used to construct a new model of the stress distributions in a peel specimen. The model is not restricted to any particular form of adherend or adhesive stress-strain behavior. The present paper describes the use of this model in conjunction with peel data to investigate failure criteria suitable to cases where adherends undergo extensive plastic deformation.

EXPERIMENTAL

Flexible-to-rigid peel joints were made with various thickness of AA5754-O aluminum sheet (1, 2, and 3 mm) bonded to a rigid aluminum plate (AA6061-T6, 12.5 mm thick) using the single-part heat-cured epoxy adhesive Betamate® 1044-3 (Essex Specialty Products Inc, Auburn Hills, MI). This combination of aluminum and adhesive were chosen to be representative of various automotive applications. The sheets (90×430 mm) and plates (90×320 mm) were degreased with acetone, washed with Alumiprep 33, and then pretreated with Alodine 5200 chrome-free conversion coating (both supplied by Henkel Corp, Brampton, ON). The sheets and plates were bonded such that a 110 mm length of sheet extended beyond the joint and could be gripped during the peel test. The bondline thickness was controlled at 0.4 mm using polytetrafluoroethylene shims, and the adhesive was cured at 180°C for at least 1 h. Each of the bonded sheet-plate joints was then cut slowly into 3 peel specimens, each 20 mm wide, using a table saw with an aqueous coolant spray. The exposure to the coolant was too brief for any appreciable absorption, and there was no evidence of edge damage on the peeled surfaces. Two batches of specimens were made, each producing 9 peel specimens (3 specimens for each of three sheet thicknesses). These two preparation batches were

TABLE 1 Average Peel Force per Unit Width (N/mm), Standard Deviation (N/mm), and Peel Length (cm) for Each Specimen Tested at 30°, 60°, and 90°

		1 mm			2 mm			3 mm		
Test		90°	60°	30°	90°	60°	30°	90°	60°	30°
1	Average	**7.12**	**12.3**	**35.3**	**9.38**	**17.2**	**50.1**	**9.25**	**18.7**	69.6
	Stnd. Dev.	**0.307**	**0.517**	**0.631**	**0.213**	**0.465**	**0.689**	**0.297**	**0.496**	0.864
	Length	**5**	**1.5**	**2.2**	**4.4**	**2.6**	**2.0**	**2.1**	**10.8**	1.9
2	Average	**6.52**	**11.9**	**35.2**	7.50	**15.3**	**47.8**	13.4	22.0	65.7
	Stnd. Dev.	**0.113**	**0.050**	**0.594**	0.783	**0.239**	**1.52**	0.107	0.379	1.46
	Length	**4.1**	**2.4**	**2.3**	2.8	**5.1**	**3.5**	4.3	5.1	2.0
3	Average	N/A	N/A	N/A	**8.67**	18.4	51.1	13.3	20.1	68.9
	Stnd. Dev.	N/A	N/A	N/A	**0.524**	0.331	1.51	0.278	1.06	1.03
	Length	N/A	N/A	N/A	**8.9**	5.8	1.7	7.1	4.6	1.5
4	Average	N/A	N/A	N/A	8.19	14.0	53.7	13.0	22.4	69.4
	Stnd. Dev.	N/A	N/A	N/A	0.317	0.307	2.54	0.134	0.333	0.969
	Length	N/A	N/A	N/A	3.5	1.6	2.1	5.5	2.7	1.2
Grand average		6.82	12.1	35.2	8.43	16.2	50.7	12.2	20.8	68.4
Stnd. Dev.		0.42	0.32	0.12	0.79	1.97	2.44	2.00	1.72	1.79

Measurements in bold indicate specimens from first preparation batch; otherwise, they belong to second preparation batch. Standard deviation in the last row corresponds to the grand average of all peel force measurements.

made of a single commercial supply batch of adhesive (Table 1 contains batch designations).

Peel tests were conducted at 30°, 60°, and 90° at 2.5 mm/min crosshead speed using the apparatus shown in Figure 1. From the first signs of adhesive failure, the peel force increased to a steady-state value as the peeling adherend was pulled into its final shape.

Tensile tests were performed on 1 mm thick cast adhesive specimens according to ASTM D638-99 [8]. Two samples from a single wafer of adhesive were tested at 0.5 mm/min loading rate. The root region of the peel joints (region around point where adhesive ruptures—see Figure 2) was photographed using a digital camera and a 40 × microscope. The curvature of the aluminum sheet at the peel root was estimated for three specimens in each of the nine steady state configurations using image processing software to fit a curve to the digitized edge of the sheet. The average standard deviation among these three repetitions was 10%. The average thickness of residual adhesive on the flexible adherend was measured using an electronic coating thickness meter (Positector 6000). Four measurements were made on each of four specimens from each of the nine peel configurations.

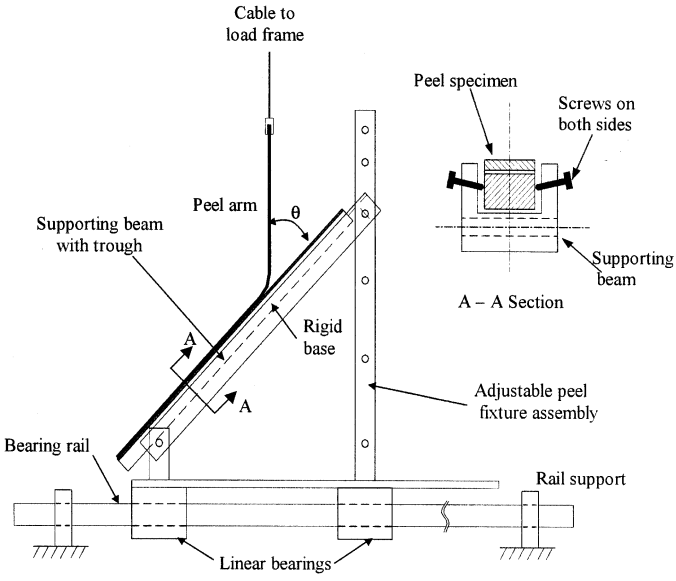

FIGURE 1 Peel apparatus.

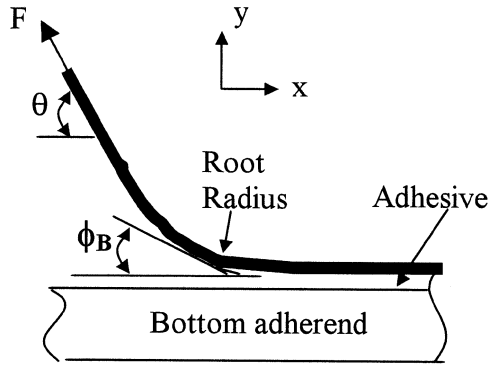

FIGURE 2 Rigid-flexible peel geometry showing steady-state peel force F, peel root radius at point B, peel angle θ, adherend root rotation ϕ_B.

RESULTS AND DISCUSSION

The Betamate 1044-3 adhesive and the AA5754-O adherend material both exhibited almost ideal elastic perfectly plastic stress-strain behavior, as illustrated in Figure 3 for the adhesive. For the adhesive, the tensile modulus was $E_a = 2.58$ GPa, while the yield stress and

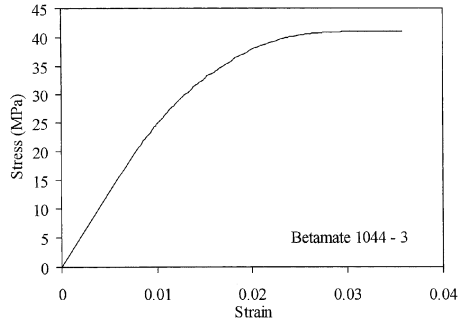

FIGURE 3 Tensile stress-strain curve for epoxy adhesive Betamate® 1044-3.

strain (0.2% offset) were $\sigma_{0.2} = 32.0\,\text{MPa}$, $\varepsilon_{0.2} = 0.014$, respectively. The adherend properties were measured to be: $E_{el} = 71.0\,\text{GPa}$, $E_{pl} = 0.483$ GPa for the elastic and plastic moduli, respectively, and $\sigma_{yp} = 100\,\text{MPa}$ for the yield stress, very close to the published values [9].

In contrast to observations of double-cantilever beam fracture tests with this adhesive [10], no obvious damage zone existed ahead of the main crack tip for all 1, 2, and 3 mm peel specimens. The crack path was always cohesive and near the flexible adherend, with the amount of residual adhesive becoming smaller with decreasing adherend thickness or increasing peel angle, as shown in Table 2. Hence, the amount of residual adhesive decreased as the peel root radius became smaller, which is equivalent to an increase in the stress concentration in the root region of the adhesive layer. This is consistent with the general observation that adhesive crack paths tend to move toward the more highly strained adherend.

Table 1 contains the peel force data for each specimen tested. The peel length represents the amount of adherend that was peeled to

TABLE 2 Thickness of Residual Adhesive Layer on Flexible Adherend after Peeling at the Given Angle; Average and Standard Deviation Based on 16 Measurements

Peel configuration	1 mm			2 mm			3 mm		
	30°	60°	90°	30°	60°	90°	30°	60°	90°
Thickness (μm)	42	38	35	52	46	38	63	55	50
Stnd. dev. (μm)	±8	±6	±4	±12	±6	±5	±15	±11	±8

obtain the corresponding average force. No significant difference was observed between the two preparation batches and so the data were pooled in subsequent analyses.

As seen in Figure 4, the average peel force decreases as the angle increases, with a much larger change occurring between 30° and 60° than between 60° and 90°. The strengthening effect of increasing adherend thickness is also much more prominent at 30° than at 90°. Both of these trends are consistent with the hypothesis that the peel strength decreases as the degree of stress concentration in the adhesive increases; *i.e.*, as the adherend load is transferred to the adhesive over a shorter zone the adherend has a greater curvature at the peel root. This is also consistent with the experimental measurements of the maximum curvature of the peeling adherend (at the root), shown in the second to last column of Table 3. Therefore, a clear relation exists between the joint strength and the degree of plastic deformation of the adherend.

Application of the Peel Model

The measured peel force for each of the nine experimental conditions was input to the model discussed in our previous article [1], and the resulting critical energy release rate G_c, and the critical von Mises strain ε_c, in the adhesive at the peel root were calculated. The corresponding curvature of the flexible adherend K_B (inverse of the radius of curvature at the peel root) and the adherend root rotation angle ϕ_B, (Figure 3) predicted by the models were also found. The critical energy

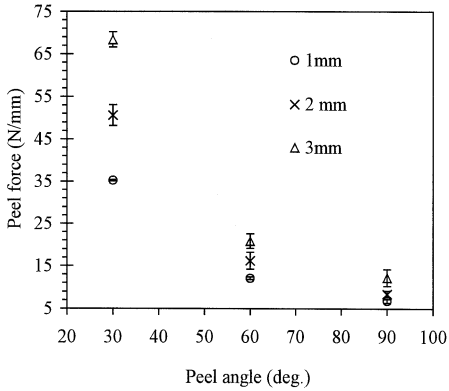

FIGURE 4 Average steady-state peel forces and standard deviations for 30°, 60°, and 90° peel tests of 1, 2, and 3 mm adherends (data of Table 1).

TABLE 3 Fracture Energy G_c Calculated Using Various Peel Models, Corresponding Calculated Root Curvature of Peeling Adherend K_B, Calculated Root Rotation ϕ_B, and Measured K_B for the Nine Peel Configurations

Peel test		Fracture energy G_c (J/m^2)				Root curvature K_B (1/mm) Root rotation ϕ_B (deg.)					
			Z				Z				
Thickness	Angle	Plane stress	plane strain	Model [4]	Uniaxial strain	Plane stress	plane strain	Model [4]	Uniaxial strain	Expt. K_B	Error (%)
1 mm	30°	2410	2150	1027	1250	0.052 8.5	0.050 7.4	0.075 2.8	0.064 3.7	0.070	−9
	60°	1310	1230	862	909	0.096 6.0	0.085 5.5	0.101 3.0	0.0903 3.5	0.082	10
	90°	1030	975	766	801	0.115 5.8	0.101 5.4	0.115 3.1	0.103 3.8	0.093	11
2 mm	30°	2210	2050	1061	1240	0.026 4.8	0.023 4.4	0.030 1.8	0.026 2.2	0.022	18
	60°	1190	1130	836	897	0.037 3.5	0.032 3.2	0.037 1.8	0.033 2.2	0.034	−3
	90°	860	834	682	723	0.040 3.2	0.035 3.0	0.039 1.8	0.035 2.2	0.035	0
3 mm	30°	2200	2120	1280	1320	0.016 3.5	0.014 3.4	0.019 1.5	0.015 1.7	0.017	−13
	60°	1350	1300	957	1050	0.022 2.9	0.019 2.7	0.022 1.5	0.019 1.8	0.020	−5
	90°	1220	1190	958	1030	0.026 3.1	0.022 2.9	0.025 1.6	0.023 2.2	0.023	0

Percentage error calculated between the curvature from uniaxial strain model ($\varepsilon_x = \varepsilon_z = 0$) and experiments.

release rate G_c was obtained as the difference between the work per unit peeled area done by the peel force F_{ext} and the energy per unit area dissipated by plastic bending in the detached peel adherend W_{pb}, using the model of Moidu et al. [4] for the peeling arm, which was incorporated into the present peel model [1]; *i.e.*, $G_c = F_{ext} - W_{pb}$. The plastic bending energy term was strongly coupled with the sandwich model through the adherend curvature and rotation at the peel root [1]. Table 3 lists these results for the plane strain model of Moidu et al. [4] and for the present model [1] under three conditions: plane stress ($\sigma_x = 0$) for both adherend and adhesive, plane strain ($\varepsilon_z = 0$) for both adherend and adhesive, and uniaxial strain ($\varepsilon_x = \varepsilon_z = 0$) for the adhesive with plane strain ($\varepsilon_z = 0$) for the adherend. As explained in

the previous paper [1], the latter model was included to generate a finite longitudinal tensile stress (σ_x) in the adhesive. The peel model of Moidu et al. [4] allowed for a bilinear plastically deforming adherend but assumed elastic adhesive behavior to failure. Nevertheless, it has been shown to give good agreement with independent experimental results [11].

The plane stress model (Table 3) predicted the largest values of G_c for each peel configuration (Figure 5) because it assumed the greatest adhesive and adherend compliance, causing ϕ_B to be relatively large and K_B to be relatively small. This decreased the plastic bending work W_{pb}, thereby increasing G_c since F_{ext} is constant for a given peel configuration. The predicted values of G_c for the nine peel configurations depend on both the values of K_B and ϕ_B predicted by the various models.

The plane strain model ($\varepsilon_z = 0$) predicts that G_c is greater than the uniaxial strain model ($\varepsilon_x = \varepsilon_z = 0$) because the adhesive is more compliant in the former, causing the root rotation to be larger, thereby decreasing W_{pb}. The predicted root curvatures of these two models are generally quite similar; however, the root rotations of the plane strain model are greater than those of the uniaxial strain model.

Of the four models, the uniaxial strain model ($\varepsilon_x = \varepsilon_z = 0$) and the model of Moidu et al. [4] agree most closely, with the predicted G_c values of the latter being consistently smaller. This is because the elastic adhesive layer assumption [4] results in greater constraint of the adherend, and hence a smaller ϕ_B and a greater K_B, both of which tend to increase W_{pb}.

A general trend among the four models is that the predicted G_c shows a much stronger dependence on peel angle, particularly between 30° and 60°, than on adherend thickness; *i.e.*, at a given peel angle, G_c is relatively constant among the three adherend thicknesses. This is the same trend seen in the peel force data of Figure 4.

Comparing the root curvature K_B predictions with the experimental measurements shows that the uniaxial strain model ($\varepsilon_x = \varepsilon_z = 0$) gives the best overall agreement with an average difference of 0.4%. The plane stress, plane strain, and model of Moidu et al. [4] differed, on average, from the experimental measurements by 8%, −5% and 16%, respectively.

The fracture energy of many adhesive joints having elastic adherends is a monotonically increasing function of the phase angle of the loading [12]. In situations where the adherends are plastically deforming, the phase angle is not well-defined and depends on the zone over which the mode I and mode II strain energies are evaluated. In the present case, an average phase angle, Ψ_{avg}, was

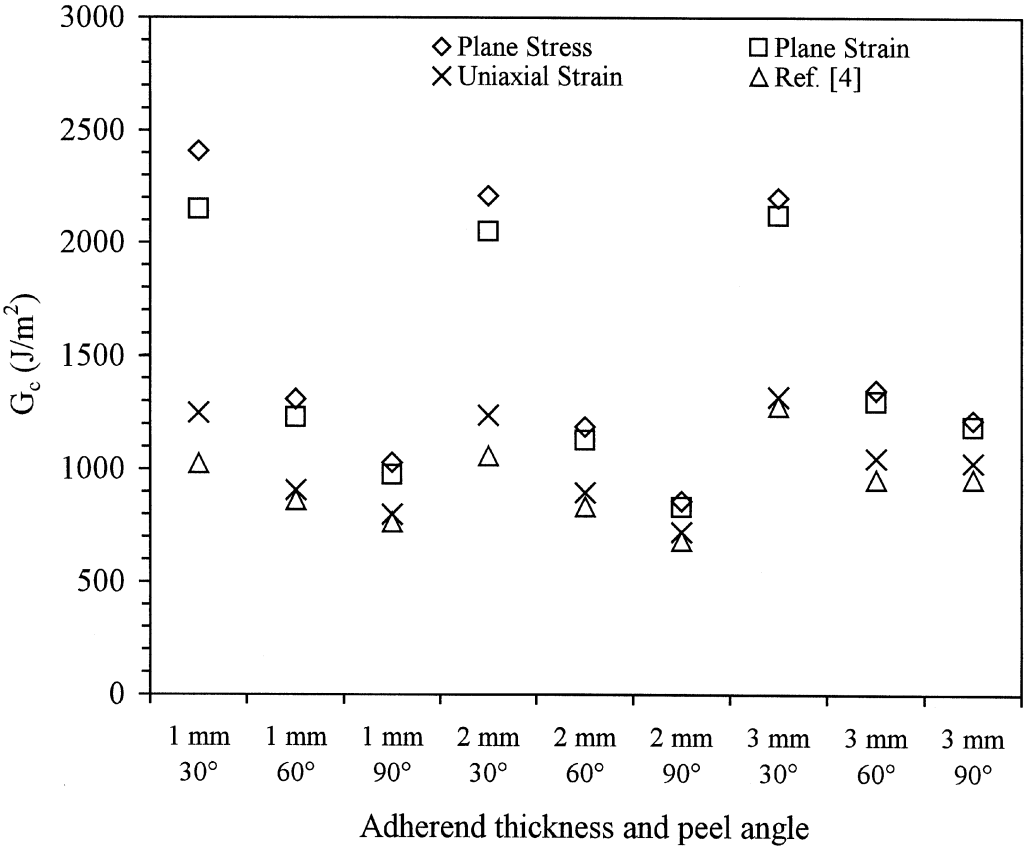

FIGURE 5 G_c for the 9 peel cases predicted by present model under conditions of plane stress, plane strain, and uniaxial strain, and model of Moidu et al. [4].

calculated as:

$$\Psi_{avg} = \arctan\left(\sqrt{\frac{\Gamma_{II}}{\Gamma_I}}\right) \tag{1}$$

where Γ_I and Γ_{II} are the tensile and shear strain energies found by integrating over the entire adhesive bondline as follows:

$$\Gamma_I = \int_0^{+\infty}\left[\int_0^{\varepsilon(x)} \frac{1}{2} E_s \varepsilon^2 d\varepsilon\right] dx \tag{2}$$

$$\Gamma_{II} = \int_0^{+\infty}\left[\int_0^{\gamma(x)} \frac{1}{2(1+\nu_p)} E_s \gamma^2 \, d\gamma\right] dx \tag{3}$$

where ε and γ are, respectively, the adhesive tensile (normal to the plane of the adhesive-adherend interface) and shear strains, while E_s and ν_p are the adhesive secant modulus and plastic Poisson ratio, respectively [1]. Equations (2) and (3) were used for calculating the phase angles for the three current models. Note that Γ_I and Γ_{II} are strain energies and not the mode I and II components of the G_c values of Table 3. Figure 6 shows the average phase angle for the 1, 2, and 3 mm specimens as a function of peel angle. It is evident that the average phase angle Ψ_{avg} is relatively insensitive to adherend thickness; the values for the three thicknesses were almost identical at a peel angle of 30°. However, Ψ_{avg} does change appreciably between 30°

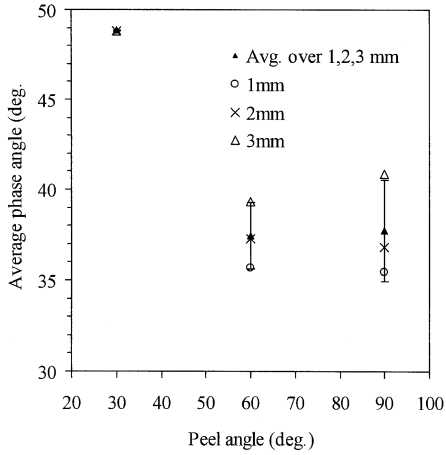

FIGURE 6 Average phase angles Ψ_{avg} and standard deviation for 1, 2, and 3 mm specimens at 30°, 60°, and and 90° peel angles.

and 60°, becoming essentially constant thereafter. Elastic double-cantilever beam fracture experiments with this same adhesive showed that at phase angles between 37° and 49°, G_c increased from approximately 2,000 J/m^2 to 3,300 J/m^2 [10]. These are again the same trends as seen in the peel force (Figure 4) and the fracture energy (Table 3); *i.e.*, a large change only between peel angles of 30° and 60°, and a negligible adherend thickness dependence. A local phase angle was also examined, based on the tensile and shear strain energies in the adhesive at the root. It was found that this measure of phase angle was erratic, being sensitive to the stress and strain at a single point, and so it varied greatly over the length of the adhesive, as shown in Figure 7 for the 3 mm 60° configuration.

Figure 8 shows the fracture energy, G_c, plotted against the average phase angle, Ψ_{avg}, for the 9 peel configurations as well as the average values for the tests grouped according to peel angle. The uniaxial strain version of the peel model was used in the calculations. To a first approximation, G_c tends to increase with Ψ_{avg}, independent of adherend thickness and peel angle over the range of these values considered in the present study.

The uniaxial strain peel model was also used to calculate the critical von Mises strain, ε_c, at the root in each of the nine peel configurations. From Figure 9, it is seen that the variation in ε_c is relatively large, and that ε_c is dependent on both the peel angle and adherend thickness; although, for the 1 and 2 mm cases, the values of ε_c at 60° and 90° are nearly the same. This strong dependence on angle and thickness implies that ε_c will not serve as a unique failure criterion for the adhesive in these situations. Similar phenomena were reported in the work of Gent and Hamad [12] and Crocombe and Adams [13], the

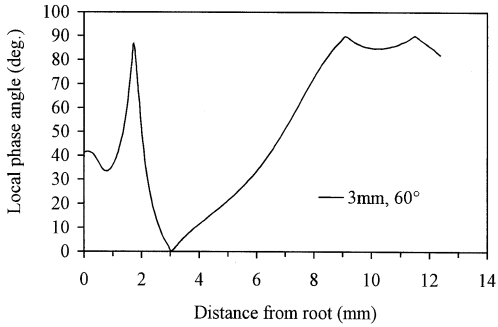

FIGURE 7 Local phase angle as a function of distance from the peel root for the 3 mm adherend at 60°.

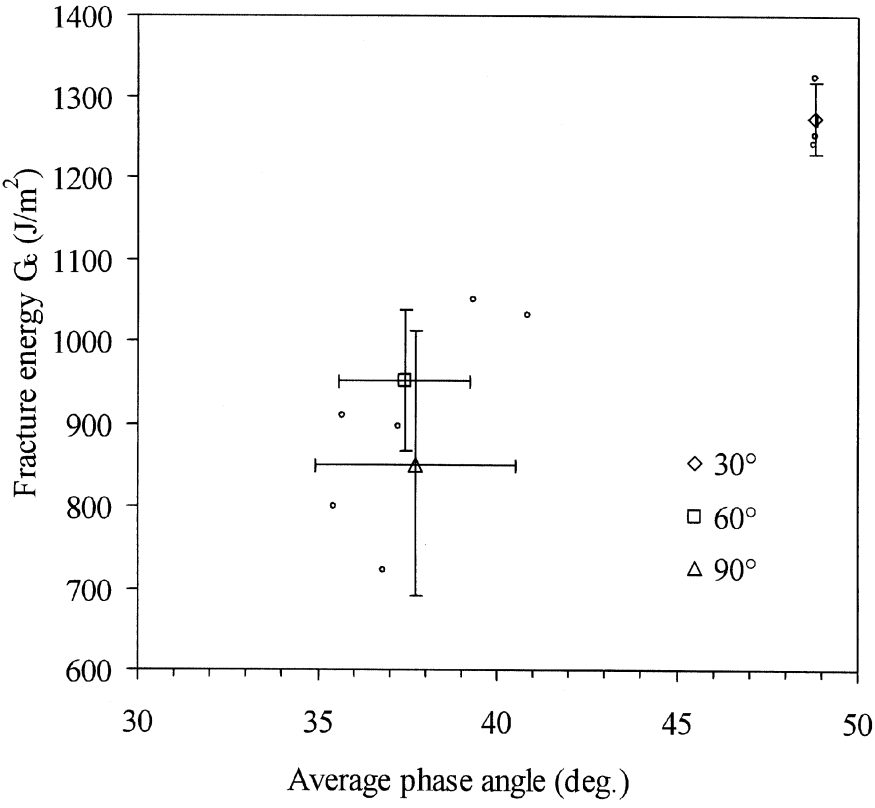

FIGURE 8 Fracture energy G_c *versus* average phase angle Ψ_{avg}, averaged over 3 sets of data—1, 2, and 3 mm adherends, each at 30°, 60°, and 90° peel angles. Error bars show the ± standard deviations in each average. Individual data points shown as (o).

latter concluding that their effective plastic strain failure criterion could be used to predict the relative peel strengths with a given adherend, but that the effective plastic strain increased with the adherend yield strength. In the present case, the von Mises critical strain increased with the adherend thickness rather than with yield strength. This implies that a factor controlling the apparent adhesive strength variation was the deformation in the adherends.

FAILURE CRITERIA

The preceding discussion focused on two potential failure criteria: the critical energy release rate G_c as a function of the average phase angle

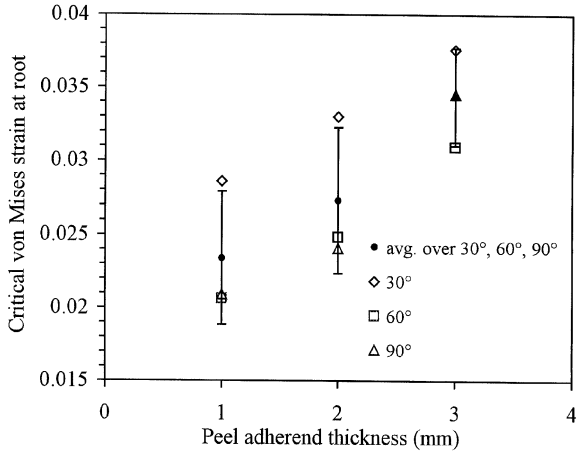

FIGURE 9 Critical von Mises strain as a function of adherend thickness for the three peel angles.

Ψ_{avg}, and the critical von Mises strain ε_c. Neither provided a unique adhesive property that was constant in all nine peel configurations, but this was not unexpected since fracture with elastic specimens also requires a two parameter criterion: G_c as a function of the phase angle of loading [14, 15]. The usefulness of these possible failure criteria, when used with the present peel model, can be judged by comparing the measured and predicted peel forces. Figure 10 does this for the uniaxial strain peel model [1] ($\varepsilon_x = \varepsilon_z = 0$) using the following two failure criteria: (1) ε_c was taken to be a function of adherend thickness alone, with the values for 1, 2, and 3 mm taken to be the averages of ε_c obtained at the three peel angles at that thickness (see Figure 9); (2) G_c was taken to be a function of Ψ_{avg} using the two available points from Figure 8, with one $G_c(\Psi_{avg})$ point representing the average of six data points at 60° and 90° for the three thicknesses ($G_c = 902\,\mathrm{J/m^2}$ at $\Psi_{avg} = 38°$), the other being the average of the three data points at 30° for the three thicknesses ($G_c = 1270\,\mathrm{J/m^2}$ at $\Psi_{avg} = 49°$). Because the average phase angle was dominated by the peel angle in the present nine peel configurations, it is noted that the latter failure criterion might also have expressed G_c as a function of peel angle rather than average phase angle. Although this would not have changed the resulting peel force prediction, it is believed that the average phase angle provides a more direct link with the mechanism of failure in the adhesive. The critical von Mises strain criterion is more restrictive than the fracture criterion, being different here for each adherend thickness.

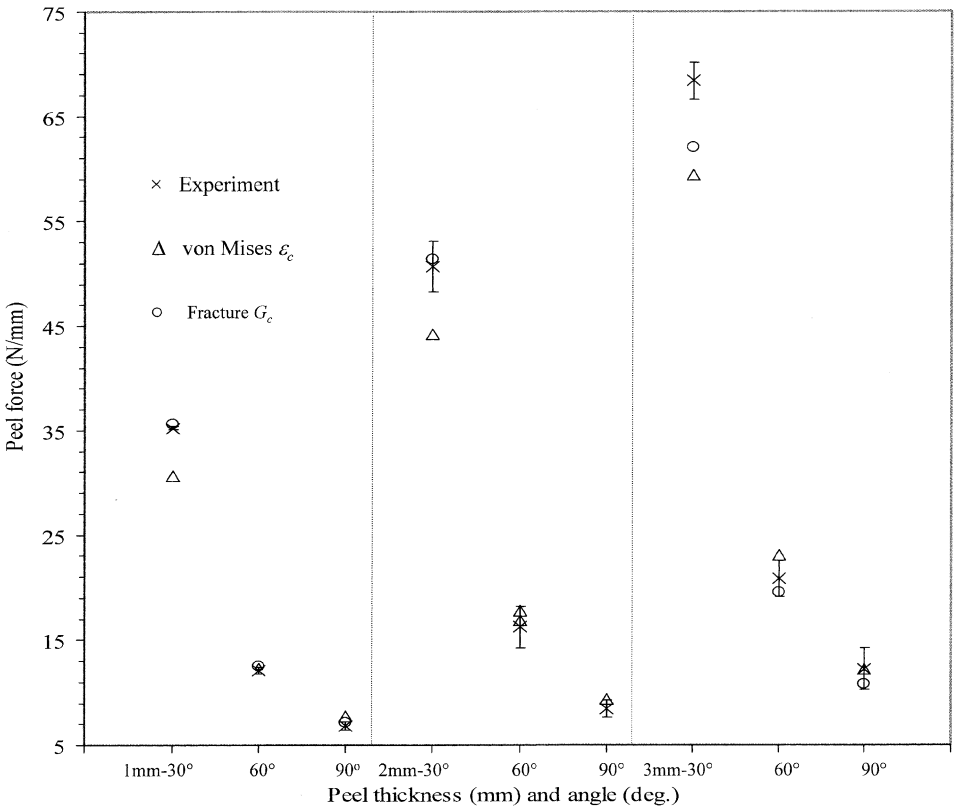

FIGURE 10 Measured peel forces and those predicted by uniaxial strain model ($\varepsilon_x = \varepsilon_z = 0$) for nine peel configurations using two different adhesive failure criteria: (1) a critical von Mises strain defined for each adherend thickness; (2) a critical energy release rate that varies with phase angle.

Figure 10 shows that both failure criteria work reasonably well in predicting the peel forces in the nine configurations. The predictions using ε_c as a function of thickness yielded an average error of 11%, with a maximum of 13%. The $G_c(\Psi_{avg})$ criterion gave an average error of 6%, with a maximum of 11%.

As mentioned above, when adhesive joint failure is accompanied by extensive adherend yielding, it is hypothesized that fracture energy should be a function of two parameters: phase angle, just as when adherends remain elastic, and some measure of the stress concentration in the adhesive layer resulting from the curvature in the adherends. Nevertheless, the fracture criterion examined in Figure 10 is apparently only a function of the phase angle averaged over the adhesive layer, without any reference to varying stress concentration. To investigate this question further, the peel model (uniaxial strain case) was used to estimate the "loading zone length" for each of the nine peel cases; *i.e.*, the distance from the peel root to the point where the von Mises stress is 15% of the yield value. The loading zone length is thus proportional to the adherend curvature. Figure 11 shows that G_c (Table 3) tends to increase as the loading zone length increases (corresponding to a decrease in the adhesive stress concentration), reaching a plateau beyond approximately 2 mm. The three longest loading zones correspond to the 30° peel angle with the 1, 2, and 3 mm adherends. This is consistent with the observation that G_c should increase with the size of the damage zone associated with a propagating crack [14, 15]. Figure 12 shows that the average phase angle also increases with the loading zone length for these same nine cases. This explains the apparent conflict with the original hypothesis; although the $G_c(\Psi_{avg})$ failure criterion does not explicitly contain a parameter expressing the degree of stress concentration imposed on the adhesive by the peel adherend, this effect is implicit in the average phase angle. Therefore, a correlation between G_c and average phase angle is also, implicitly, a correlation with the degree of stress concentration imposed by the adherend.

The fracture energies measured in these peel tests were much smaller than those measured with elastic DCB specimens [10] by a factor of approximately 2.5: $G_c = 902\,\mathrm{J/m^2}$ compared with 2,000 $\mathrm{J/m^2}$ at $\Psi_{avg} = 38°$, and $G_c = 1,270\,\mathrm{J/m^2}$ compared with 3,300 $\mathrm{J/m^2}$ at $\Psi_{avg} = 49°$. This is due to the increasing size of the adhesive loading zone as the adherends become thicker. As mentioned above, steady-state fracture in elastic DCBs with this adhesive system was characterized by a damage zone extending several millimeters ahead of the macroscopic crack tip. This is similar to the behavior of other toughened epoxy adhesives in these tests [15]. Thus, as the adherends

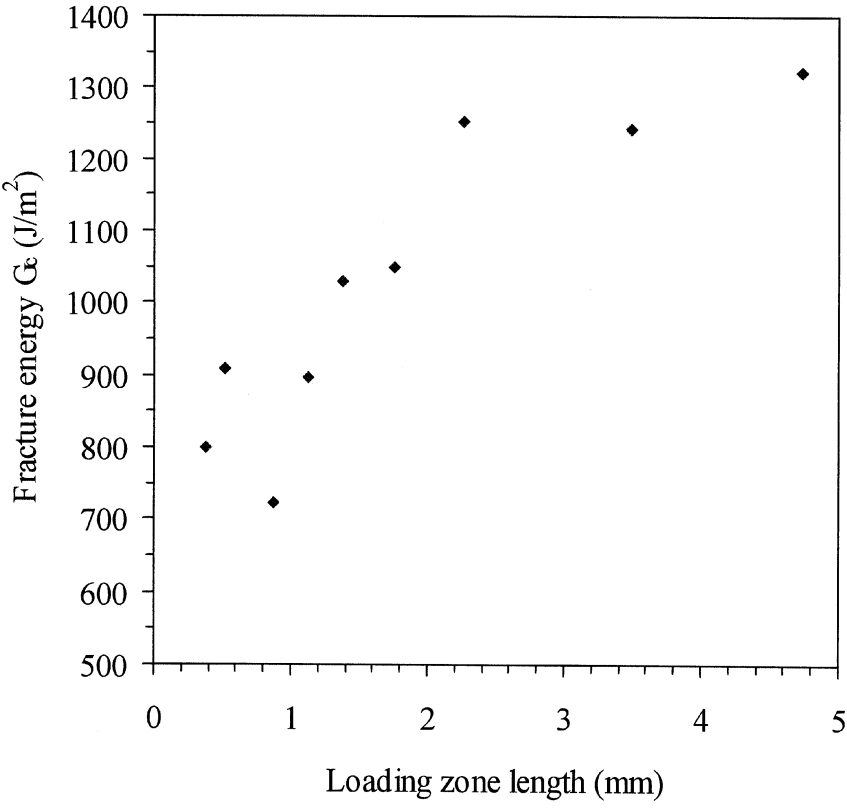

FIGURE 11 Fracture energy G_c as a function of loading zone length for 1, 2, and 3 mm adherends peeled at 30°, 60°, and 90°.

become more rigid, a greater volume of adhesive is involved in the fracture process and the critical energy release rate increases.

CONCLUSIONS

The analytical peel model, developed in previous research [1] from a general sandwich model, was evaluated using experimental measurements of steady state peel force and adherend curvature for 1, 2, and 3 mm adherends, each peeled at 30°, 60°, and 90°. Two adhesive failure criteria were examined: critical von Mises strain ε_c and critical fracture energy G_c. A single value of ε_c did not exist, but the model provided reasonably accurate predictions of the peel force (average error of 11%) if the dependence on peel angle was ignored; *i.e.*, ε_c was

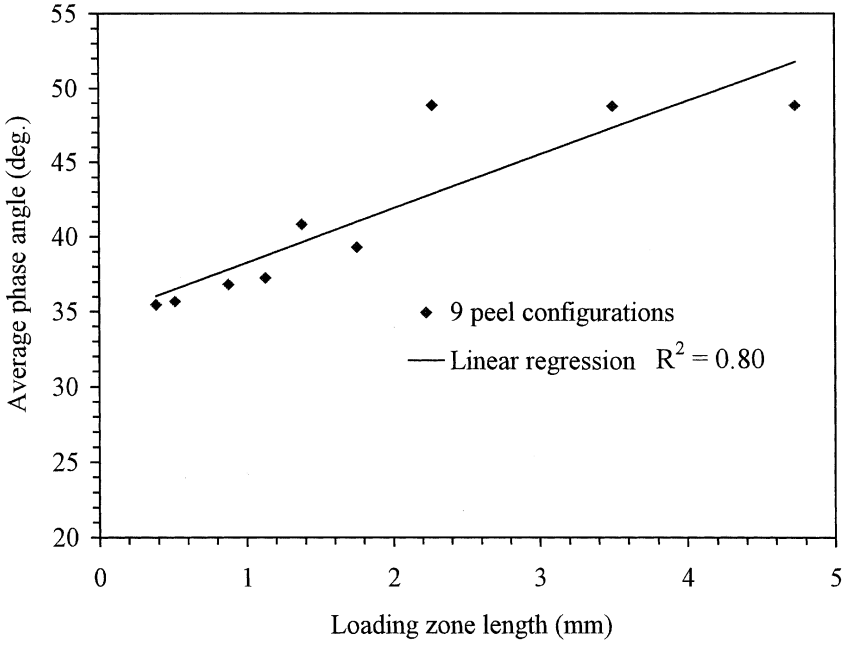

FIGURE 12 Average phase angle Ψ_{avg} as a function of damage zone length for 1, 2, and 3 mm adherends peeled at 30°, 60°, and 90°.

taken to vary only with adherend thickness. G_c could be taken as a function of the average phase angle that depended primarily on the peel angle. This criterion yielded predicted peel forces having an average error of 6%. The average phase angle has a direct correlation with the loading zone length in the adhesive, and therefore has an implicit relation with the degree of stress concentration imposed on the adhesive by the peeling adherend. Since the underlying sandwich model is generic, these results should be applicable to joint geometries other than the present flexible-rigid configuration. Following the present procedure, the sandwich model can, in principle, be coupled to adherend models for a variety of two-dimensional adhesive joints that fail with extensive adherend yielding.

REFERENCES

[1] Wang, R., Cui, J., Sinclair, A. N., and Spelt, J. K., "Strength of Adhesive Joints with Adherend Yielding: I – Analytical Model," *J. Adhesion* **79**, 23–48 (2003).
[2] Crocombe, A. D., and Adams, R. D., *J. Adhesion* **13**, 241–267 (1982).
[3] Kinloch, A. J., Lau, C. C., and Williams, G. J., *Int. J. Fracture* **66**, 45–70 (1994).

[4] Moidu, A. K., Sinclair, A. N., and Spelt, J. K., *J. Testing and Evaluation* **26**, 247–254 (1998).
[5] Kinloch, A. J., and Hadavina, H., *Proc. 23rd Annual Meeting of the Adhesion Society*, Myrtle Beach, South Carolina, pp. 25–28 (2000).
[6] Yang, Q. D., Thouless, M. D., and Ward, S. M., *J. Mechanics Physics Solids* **47**, 1337–1353 (1999).
[7] Wei, Y., and Hutchinson, J. W., *Int. J. Fracture* **93**, 315–333 (1998).
[8] ASTM D638-99, "Standard Test Method for Tensile Properties of Plastics," American Society for Testing and Materials, West Conshohocken, PA (1999).
[9] ASTM B209 M-95, "Aluminum and Magnesium Alloys," American Society for Testing and Materials, West Conshohocken, PA (1995).
[10] Cui, J., *Finite Element Modeling of Adhesive Failure with Adherend Yielding*, MASc. Thesis, Department of Mechanical and Industrial Engineering, University of Toronto (2001).
[11] Price, A. J., and Sargent, J. P., *Int. J. Adhesion Adhesives* **17**, 27–32 (1997).
[12] Gent, A. N., and Hamed, G. R., *J. of Appl. Polymer Sci*. **21**, 2817–2831 (1997).
[13] Crocombe, A. D., and Adams, R. D., *J. Adhesion* **12**, 127–139 (1981).
[14] Fernlund, G., and Spelt, J. K., *J. Composites Tech. Research* **16**, 234–243 (1994).
[15] Papini, M., Fernlund, G., and Spelt, J. K., *Composites Sci. and Tech*. **52**, 561–570 (1994).